Magnetic structure and exchange interactions of transition metal dihalide monolayers: First-principles studies

Xiangyan Bo,[1] Lei Fu,[1] Xiangang Wan,[2,3] Shasha Li,[1,*] and Yong Pu[1,†]

[1]*New Energy Technology Engineering Laboratory of Jiangsu Province & School of Science, Nanjing University of Posts and Telecommunications, Nanjing 210023, China*

[2]*National Laboratory of Solid State Microstructures and School of Physics, Nanjing University, Nanjing 210093, China*

[3]*Collaborative Innovation Center of Advanced Microstructures, Nanjing University, Nanjing 210093, China*

(Received 17 July 2023; revised 2 October 2023; accepted 18 December 2023; published 8 January 2024)

Based on the first-principles linear response method and Monte Carlo simulation, we investigate the magnetic properties of single-layer transition metal dihalides MX_2 (M = V, Cr, Mn, Fe, Co, Ni; X = Cl, Br, I). We calculate the magnetic exchange interactions using the first-principles linear response method and find that the third-nearest-neighbor interaction of most dihalides is very important. When spin-orbit coupling is included, FeX_2 and CrX_2 (X = Cl, Br, I) are predicted to be insulators. Using the parameters of the exchange interactions and magnetic anisotropy, the magnetic ground states of transition metal dihalide monolayers are obtained by Monte Carlo simulation. Moreover, we find that the magnetic ground states of ten MX_2 monolayers are independent of the U value. Among them, the magnetic ground state of CrI_2 is ferromagnetic, the magnetic ground state of $CrCl_2$ is collinear antiferromagnetic, the magnetic ground states of VCl_2, FeI_2, and CoX_2 (X = Br, I) are 120° antiferromagnetic, and the magnetic ground states of $FeCl_2$ and NiX_2 (X = Cl, Br, I) are helimagnetic.

DOI: 10.1103/PhysRevB.109.014405

I. INTRODUCTION

Since the successful synthesis of atomically thin CrI_3 [1], $Cr_2Ge_2Te_6$ [2], and Fe_3GeTe_2 [3], two-dimensional (2D) van der Waals (vdW) magnetic materials have attracted extensive attention. These intrinsically magnetic 2D vdW magnets provide an ideal platform for exploring long-range magnetic ordering at the 2D limit and show promising applications in next-generation spintronics devices. However, few 2D vdW materials have been synthesized experimentally so far. Therefore first-principles calculations have attracted more and more attention in the search for 2D magnetic materials, and a large number of 2D magnetic materials have been predicted, such as transition metal halides (MX_3 and MX_2, where M is a transition metal and X = Cl, Br, I) [4–8], transition metal dichalcogenides (MX_2, where M is a transition metal and X = O, S, Se, Te) [9–11], ternary transition metal compounds (ABX_3, where A and B are metal cations and X is an anion) [12–16], etc.

The single-layer transition metal dihalides have been shown to be stable in previous studies [4]. The calculation of the formation energy of transition metal dihalides confirmed that their monolayers are not only stable but also potentially exfoliable [4]. In recent years, single-layer 3d transition metal dihalides MX_2 have attracted increasing attention [17–22]. Although some advancements have been made in the study of 3d transition metal dihalide monolayers, there are still many issues that require in-depth investigation: (i) At present, magnetic analysis of monolayer MX_2 is mainly focused on collinear magnetic ordering. However, since the transition metal atomic arrangements of monolayer MX_2 are triangular lattices, the geometric frustration of the spin configurations is inevitable. For example, many experimental [23–26] and theoretical [21,22,27] works show that the ground state magnetic order of NiI_2 is helimagnetic. However, some other theoretical studies only consider the nearest-neighbor interaction and predict that the magnetic ground state of monolayer NiI_2 is ferromagnetic (FM) [4,6,28]. (ii) Many theoretical studies have predicted a half-metallic state of monolayer $FeCl_2$ with a large spin gap [20,29–31]. In fact, however, Cai *et al.* demonstrated that monolayer $FeCl_2$ is a uniform insulator with a gap of the magnitude of an electron volt [32]. Recently, Lu *et al.* [33] obtained a FM insulator solution by properly treating the spin-orbit coupling (SOC), but the estimated Curie temperature (T_C = 25 K) is much smaller than that of previous works (109–470 K) [4,6,20]. As a result, accurate prediction of magnetic properties of MX_2 requires the correct electron ground state and magnetic exchange Hamiltonian. The determination of the magnetic ground state of MX_2 is still a significant problem.

In this paper, based on density functional theory (DFT), we systematically study the magnetic properties of single-layer 3d transition metal dihalides MX_2 (M = V, Cr, Mn, Fe, Co, Ni; X = Cl, Br, I). We calculate the magnetic exchange constants based on the combining magnetic force theorem and linear response approach [34–37] and find that the third-nearest-neighbor interaction J_3 is crucial for most dihalides. When SOC is included, we estimate the magnetic anisotropy energy (MAE) and find that monolayer FeX_2 and CrX_2 (X = Cl, Br, I) change from semimetals to insulators. With the calculated magnetic exchange constants and MAE, we carry out Monte Carlo simulations and determine the magnetic phase diagram.

*shashali@njupt.edu.cn
†puyong@njupt.edu.cn

We find that when $U = 2$ eV, only the magnetic ground state of monolayer CrI_2 is FM and its Curie temperature is 100 K. In addition, we also study the magnetic ground states of dihalide monolayers with different U values and find that the magnetic ground states of VX_2 (X = Br, I), $CrBr_2$, MnX_2 (X = Cl, Br, I), $FeBr_2$, and $CoCl_2$ depend on the value of the Hubbard U.

II. METHOD

The electronic structure calculations were carried out by using the full potential linearized augmented plane-wave method as implemented in the WIEN2K package [38]. For the exchange-correlation potential, the generalized gradient approximation (GGA) is used for structural relaxation and optimization. The crystal structure of monolayer MX_2 is fully optimized, while the vacuum space is set to be 15 Å to avoid interactions with other neighboring layers. GGA + U calculations are performed to include the effect of Coulomb repulsion in the 3d orbital [39]. We also consider various values of the effective parameter U_{eff} ($U_{\text{eff}} = 2$–6 eV). $U = 2$ eV is used in the following calculations, while the results of other U values are provided in the Supplemental Material [40]. Using the second-order variational procedure, we include the SOC interaction [41]. The basic functions were expanded to $R_{mt} \times K_{\max} = 7$, where R_{mt} is the smallest of the muffin-tin sphere radii and $K_{\max}$ is the largest reciprocal lattice vector used in the plane-wave expansion. A $15 \times 15 \times 1$ k-point mesh is used for the Brillouin zone integral. The convergence of k-point meshes has been tested to ensure the accuracy of magnetic exchange constants. The self-consistent calculations are considered to be converged when the difference in the total energy of the crystal does not exceed 0.001 mRy at consecutive steps.

The magnetic exchange interactions are the basis for understanding the magnetic properties, and the first-principles calculation of exchange constants has attracted much interest. Commonly used methods include energy-mapping analysis [42] and the spin-polarized Ruderman-Kittel-Kasuya-Yosida (RKKY) method [34,43–46]. Here, we use the method based on combining the magnetic force theorem and the linear response approach [34–37] to calculate the exchange interactions. The magnetic force theorem [34] assumes a rigid rotation of atomic spin at sites $R + \tau$ and $R' + \tau'$ of the lattice (here R are the lattice translations, and τ are the atoms in the basis). Then, the exchange constant J can be given as a second variation of the total energy induced by the rotation of atomic spin at sites $R + \tau$ and $R' + \tau'$ [35],

$$J^{\alpha\beta}_{R_l+\tau,R_{l'}+\tau'} = \sum_{nkn'k'} \frac{f_{nk} - f_{n'k'}}{\varepsilon_{nk} - \varepsilon_{n'k'}} \langle \psi_{nk} | [\sigma \times B_\tau]_\alpha | \psi_{n'k'} \rangle \times \langle \psi_{n'k'} | [\sigma \times B_{\tau'}]_\beta | \psi_{nk} \rangle e^{i(k'-k)(R_l - R_{l'})}, \quad (1)$$

where σ and B are the Pauli matrix and the effective local magnetic field, respectively. ε is the one-electron energy, while ψ is the corresponding wave function. n represents the band index, and k represents the k point index. This method directly computes the lattice Fourier transform $J(q)$ of the exchange interaction $J(R_l)$ and is convenient to obtain the exact long-range exchange interactions. This technique has been successfully applied to evaluate magnetic interactions in various magnetic materials [35–37,47–53. The algorithm of this method is now implemented in open-source software called WIENJ [54], as an interface to WIEN2K [38]. Based on the calculated magnetic exchange interactions, we explore the magnetic phase diagrams by a replica-exchange Monte Carlo method [8,55].

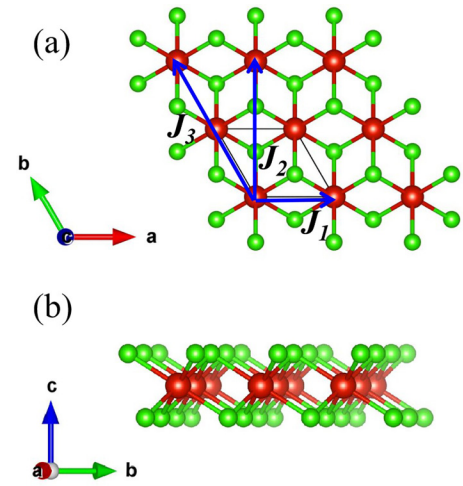

FIG. 1. (a) Top and (b) side views of the single-layer transition metal dihalide MX_2. The red and green balls represent the M and X ions, respectively. The arrows define the magnetic exchange interactions.

III. RESULTS AND DISCUSSION

A. Crystal structure

Transition metal dihalide monolayers have two common crystal structures, namely the 2H phase with P-6m2 space group and the 1T phase with P-3m1 space group. Previous studies have demonstrated that all monolayer MX_2 (M = V, Cr, Mn, Fe, Co, Ni; X = Cl, Br, I) tend to have 1-T structures at the monolayer level [4,7]. Therefore here we will focus only on the 1-T phase. The typical crystal structure of monolayer MX_2 is shown in Fig. 1. For a 2D vdW system, careful treatment of long-range interactions is essential [56]. Since monolayer MX_2 does not involve interlayer interactions, we do not consider the vdW interaction here, and we use the GGA scheme for structural relaxation and optimization as in previous studies [4,6]. The calculated lattice parameters of

TABLE I. Calculated lattice parameters (in angstroms) for monolayer MX_2 within the GGA scheme.

a	Cl	Br	I
V	3.65	3.83	4.11
Cr	3.64	3.82	4.09
Mn	3.70	3.88	4.15
Fe	3.53	3.73	4.02
Co	3.52	3.73	3.97
Ni	3.49	3.68	3.96

TABLE II. The magnetic exchange constants (in meV) of monolayer MX_2 (M = V, Cr, Mn, Fe, Co, Ni; X = Cl, Br, I) evaluated from the GGA + U (U = 2 eV) scheme. The calculated band gaps (in eV) and magnetic moments (in μ_B) are presented in the second and third columns. HM, half metal.

	Gap	m	J_1	J_2	J_3
VCl_2	2.55	2.70	4.91	0.03	0.21
VBr_2	2.41	2.72	1.79	0.07	0.33
VI_2	2.29	2.73	−2.19	0.15	0.48
$CrCl_2$	HM	3.76	1.22	−0.41	−6.40
$CrBr_2$	HM	3.80	−0.59	−0.65	−7.81
CrI_2	HM	3.85	−2.48	−1.05	−8.90
$MnCl_2$	2.94	4.62	1.50	0.08	0.22
$MnBr_2$	2.61	4.60	1.18	0.13	0.32
MnI_2	2.00	4.57	0.92	0.25	0.45
$FeCl_2$	HM	3.65	−14.74	−0.17	−0.36
$FeBr_2$	HM	3.62	−11.48	−0.43	−0.35
$FeI2_2$	HM	3.55	−7.18	−0.70	−0.13
$CoCl_2$	1.87	2.62	0.48	0.07	0.74
$CoBr_2$	1.50	2.58	1.46	0.07	1.20
CoI_2	0.87	2.46	4.00	0.05	2.61
$NiCl_2$	1.93	1.55	−1.13	0.0008	1.38
$NiBr_2$	1.46	1.48	−0.95	−0.006	2.38
NiI_2	0.88	1.35	−0.68	0.0003	4.76

monolayer MX_2 are shown in Table I and are consistent with theoretical and experimental bulk material data [4,6].

B. Magnetic properties

Based on the optimized crystal structure, we perform GGA + U (U = 2 eV) calculations with the FM configuration. The calculated band gaps and magnetic moments on the transition metal ions are shown in Table II. The results indicate that monolayer CrX_2 and FeX_2 (X = Cl, Br, I) are half metals while other dihalide monolayers are insulators, which is consistent with previous theoretical studies [6]. The calculated magnetic moments of M^{2+} ions are in agreement with the previous theoretical results [4,6], indicating the high spin state of M^{2+} ions.

As shown in Fig. 1, we depict the main magnetic interactions. Based on the calculated FM structure, we estimate the magnetic exchange constants for the first-nearest neighbor J_1, the second-nearest neighbor J_2, and the third-nearest neighbor J_3 in Table II. We also calculate the exchange interactions of the fourth and more distant neighbors, and as shown in Fig. S2 of the Supplemental Material [40], the exchange constants decrease rapidly with increasing distance. It can be seen from Table II that most dihalide monolayers have relatively strong J_3, including MCl_2 (M = Cr, Co, Ni), MBr_2 (M = Cr, Mn, Co, Ni), and MI_2 (M = Cr, Mn, Co, Ni). The J_1, J_2, and J_3 of CrX_2 (X = Br, I) and FeX_2 (X = Cl, Br, I) are FM; so their magnetic ground states are FM, and the results for FeX_2 (X = Cl, Br, I) are consistent with previous theoretical calculations [4,6,7]. In contrast, the J_1 and J_3 of the eight dihalides are antiferromagnetic (AFM), and their magnetic ground states should be AFM, including VX_2 (X = Cl, Br), MnX_2 (X = Cl, Br, I), and CoX_2 (X = Cl, Br, I). In addition, VI_2, $CrCl_2$, and NiX_2 (X = Cl, Br, I) have different signs for J_1 and J_3, and the magnetic ground states need to be determined by Monte Carlo simulations.

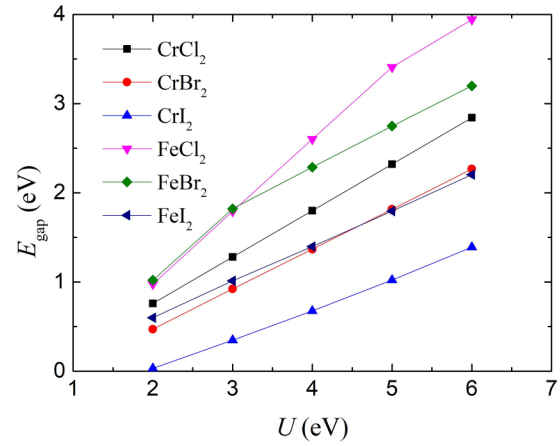

FIG. 2. The calculated band gaps of monolayer MX_2 (M = Cr, Fe; X = Cl, Br, I) evaluated from the GGA + SOC + U scheme.

C. SOC and MAE

It is worth mentioning that although monolayer $FeCl_2$ was predicted to be a semimetal in previous theoretical studies [20,29–31], experiments demonstrated that it is a uniform insulator with a gap of 1.2 eV [32]. Recent theoretical studies have shown that SOC can lead to metal-insulator transitions for $FeCl_2$ [6,33,57]. Therefore we also perform GGA + SOC + U calculations for monolayer CrX_2 and FeX_2 (X = Cl, Br, I) and find that they are all insulators. The calculated band gaps of monolayer CrX_2 and FeX_2 (X = Cl, Br, I) are shown in Fig. 2. The band gap of $FeCl_2$ calculated by the GGA + SOC + U (U = 2 eV) scheme is 0.98 eV, which is close to the experimental value (1.2 eV) [32]. Moreover, we also use the Vienna *ab initio* simulation package (VASP) with the revised Heyd-Scuseria-Ernzerhof (HSE06) hybrid functional to get a more accurate electronic structure prediction of monolayer $FeCl_2$ and obtain a band gap of 3.4 eV. The calculation details and results are described in Secs. A and C of the Supplemental Material [40].

Using the first-principles linear response (FPLR) method, we also calculate the exchange interactions including SOC. We find that the exchange couplings of monolayer CrX_2 and FeX_2 (X = Cl, Br, I) change significantly due to the opening of a band gap as a result of the metal-insulator transition, while the exchange constants of other dihalide monolayers change little (less than 0.01 meV). It can be seen from Table III that after SOC is included, the J_1 of $CrBr_2$ changes from FM to AFM, while the values of J_2 and J_3 of CrX_2 (X = Cl, Br, I) are much smaller. For FeX_2 (X = Cl, Br, I), all exchange interactions change from FM to AFM except for J_1 of $FeCl_2$. Our J_1 of $FeCl_2$ (−0.92 meV) agrees well with the results of other calculations (−0.7 meV) [19,33].

To determine the MAE, we perform GGA + SOC + U calculations with spin orientations perpendicular to the *ab* plane and lying in the *ab* plane, i.e., the spin orientations are along the (001) and (100) directions. We list the calculated

TABLE III. The magnetic exchange constants (in meV) of monolayer MX_2 (M = Cr, Fe; X = Cl, Br, I) evaluated from the GGA + SOC + U (U = 2 eV) scheme. The calculated band gaps (in eV) and magnetic moments (in μ_B) are presented in the second and third columns.

	Gap	m	J_1	J_2	J_3
$CrCl_2$	0.76	3.71	3.01	0.02	−0.73
$CrBr_2$	0.47	3.75	0.73	0.006	−1.25
CrI_2	0.03	3.79	−1.29	−0.07	−2.59
$FeCl_2$	0.98	3.64	−0.92	0.11	0.36
$FeBr_2$	1.02	3.61	0.10	0.13	0.56
FeI_2	0.60	3.55	1.50	0.27	0.98

MAE in Table IV and find that the MAEs of monolayer CrX_2 and FeX_2 (X = Cl, Br, I) are very large (even larger than the exchange constant). For $FeCl_2$, the (001) direction has a higher energy (36 meV) than the (100) direction, consistent with previous theoretical calculations (55 meV) [19]. We also use VASP to confirm the results of magnetic anisotropy, and the calculation results are listed in Table S8 in the Supplemental Material [40]. Our calculations show that the (001) direction of CrX_2 (X = Cl, Br, I), MnI_2, and NiI_2 is the easy axis, while the (001) direction of FeX_2 (X = Cl, Br, I), CoX_2 (X = Cl, Br, I), and $NiCl_2$ is the hard axis. In addition, VX_2 (X = Cl, Br, I), MnX_2 (X = Cl, Br), and $NiBr_2$ have different easy axis directions calculated by WIEN2K and VASP.

It is worth mentioning that due to the inversion symmetry, $J_{ij}^{\alpha\beta} = J_{ij}^{\beta\alpha}$, there is no Dzyaloshinskii-Moriya interaction in monolayer MX_2. Considering the potential significance of higher-order interactions in layered magnetic materials [58], we investigate the biquadratic exchange interactions of some monolayer dihalides in Sec. H of the Supplemental Material [40]. The biquadratic exchange of MCl_2 (M = V, Cr, Mn, Fe, Co, Ni) calculated from noncollinear DFT simulations by VASP is shown in Table S10.

TABLE IV. MAE (in meV) of monolayer MX_2 (M = V, Cr, Mn, Fe, Co, Ni; X = Cl, Br, I) with different U values. When no value is given, this indicates that the calculated MAE is less than 0.01 meV.

	U = 2 eV	U = 4 eV	U = 6 eV
VCl_2	−0.04	−0.07	−0.09
VBr_2	−0.04		
VI_2			−0.03
$CrCl_2$	3.06	1.63	1.01
$CrBr_2$	6.16	3.58	2.24
CrI_2	10.9	10.6	7.68
$MnCl_2$	−0.23	−0.22	−0.23
$MnBr_2$			
MnI_2	0.57	0.58	0.53
$FeCl_2$	−36.0	−40.8	−40.1
$FeBr_2$	−35.4	−37.8	−36.1
FeI_2	−36.0	−37.0	−34.1
$CoCl_2$	−0.13	−0.10	−0.08
$CoBr_2$	−0.66	−0.49	−0.34
CoI_2	−1.16	−0.95	−0.68
$NiCl_2$	−0.03	−0.03	−0.03
$NiBr_2$	0.03		0.04
NiI_2	0.66	0.57	0.36

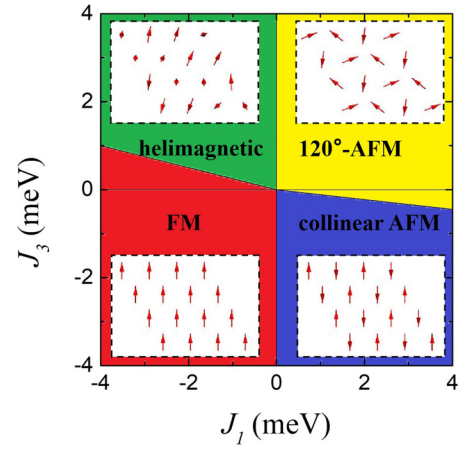

FIG. 3. The phase diagram obtained by the Monte Carlo simulations. The insets show schematic diagrams of the spin configuration.

D. Magnetic ordering

Based on the calculated magnetic exchange constants, we use the following Heisenberg model and carry out Monte Carlo simulations to estimate the magnetic transition temperature and the magnetic phase diagram for monolayer MX_2:

$$H = \sum_{i<j} J_{ij} S_i \cdot S_j - \sum_i A\left(S_i^z\right)^2, \tag{2}$$

where A is the MAE. S_i is the spin vector (of unit length) at site i. We adopt $L \times L \times 1$ supercells with $L = 36$ in our Monte Carlo simulations.

Since most dihalides have very small values for J_2, and to simplify the model, we first set $J_2 = 0$ and $A = 0.1$ meV in the following simulations. Subsequently, we obtain the magnetic phase diagram of J_1 and J_3 in Fig. 3. As expected, when both J_1 and J_3 are negative, the magnetic ground state is FM; when both J_1 and J_3 are positive, the magnetic ground state is 120° AFM; when $J_1 < 0$ and $J_3 > 0$, if $J_3 < |J_1|/4$, the magnetic ground state is FM, and otherwise the magnetic ground state is helimagnetic [59,60]; and when $J_1 > 0$ and $J_3 < 0$, if $|J_3| < J_1/9$, the magnetic ground state is 120° AFM, and otherwise the magnetic ground state is collinear AFM. Therefore the magnetic ground states of VX_2 (X = Cl, Br), MnX_2 (X = Cl, Br, I), and CoX_2 (X = Cl, Br, I) are 120° AFM. For the five dihalides with different signs of J_1 and J_3 by the GGA + U (U = 2 eV) scheme, VI_2 is FM, $CrCl_2$ is collinear AFM, and NiX_2 (X = Cl, Br, I) are helimagnetic. Furthermore, when SOC is included, CrX_2 (X = Cl, Br) are collinear AFM, CrI_2 is FM, $FeCl_2$ is helimagnetic, and FeX_2 (X = Br, I) are 120° AFM.

Next, we also perform Monte Carlo simulations using the value of A given in Table IV for the model containing J_2. The obtained magnetic ground states are summarized in the second column of Table V. The results show that the magnetic ground state of VI_2 changes from FM to helimagnetic, and the

TABLE V. Magnetic ground state of monolayer MX_2 from Monte Carlo simulations with different U values. FM, FM state; AFM, collinear AFM state; 120, 120° AFM state; H, helimagnetic state. The magnetic ground states of monolayer CrX_2 and FeX_2 (X = Cl, Br, I) including SOC are shown in parentheses.

	$U = 2$ eV	$U = 4$ eV	$U = 6$ eV
VCl_2	120	120	120
VBr_2	120	120	H
VI_2	H	FM	FM
$CrCl_2$	AFM (AFM)	FM (AFM)	FM (AFM)
$CrBr_2$	FM (AFM)	FM (FM)	FM (FM)
CrI_2	FM (FM)	FM (FM)	FM (FM)
$MnCl_2$	120	120	H
$MnBr_2$	120	H	H
MnI_2	120	FM	FM
$FeCl_2$	FM (H)	FM (H)	FM (H)
$FeBr_2$	FM (H)	FM (120)	FM (H)
FeI_2	FM (120)	FM (120)	FM (120)
$CoCl_2$	120	120	H
$CoBr_2$	120	120	120
CoI_2	120	120	120
$NiCl_2$	H	H	H
$NiBr_2$	H	H	H
NiI_2	H	H	H

magnetic ground state of $FeBr_2$ changes from 120° AFM to helimagnetic.

With the calculated magnetic exchange constants and anisotropy energy, we also simulate the thermal dependence of magnetic properties and the magnetic transition temperature. Figure 4 depicts the magnetization and magnetic susceptibility as functions of temperature for CrI_2, the only FM insulator at $U = 2$ eV. The calculated magnetic transition temperature of CrI_2 is 100 K.

E. The influence of Hubbard U

As changes in U can modify the magnetic states and properties of $3d$ metal compounds, theoretically it is necessary to calculate the value of U for each material [61,62]. Here, we have varied the value of U from 2.0 to 6.0 eV, and the calculated magnetic exchange constants of $U = 4$ and 6 eV are provided in Tables S4, S5, S6, and S7 in the Supplemental Material [40]. As shown in Table IV, changing U has little effect on the MAE and does not change the easy axis. Moreover, we also investigate the effect of different U values on the magnetic ground state. It can be seen from Table V that VX_2 (X = Br, I), $CrBr_2$, MnX_2 (X = Cl, Br, I), $FeBr_2$, and $CoCl_2$ will change the magnetic ground state with different U values. Among them, when the value of U increases above 4 eV, the magnetic ground states of VI_2, $CrBr_2$, and MnI_2 become FM.

IV. CONCLUSIONS

In conclusion, the magnetic properties of single-layer transition metal dihalides are further studied based on the magnetic interaction calculated by the first-principles linear response method. When spin-orbit coupling is handled properly, monolayer FeX_2 and CrX_2 (X = Cl, Br, I) change from half metals to insulators. Based on the obtained magnetic exchange constants and anisotropy energy, Monte Carlo simulations are performed, and magnetic phase diagrams are generated. The results indicate that when $U = 2$ eV, only the magnetic ground state of monolayer CrI_2 is ferromagnetic and its Curie temperature is 100 K. Moreover, there are ten dihalide monolayers whose magnetic ground states do not depend on the value of the Hubbard U. In addition to CrI_2 having a ferromagnetic ground state, $CrCl_2$ has a collinear antiferromagnetic ground state; VCl_2, FeI_2, and CoX_2 (X = Br, I) have 120° antiferromagnetic ground states; and $FeCl_2$ and NiX_2 (X = Cl, Br, I) have helimagnetic ground states. These results emphasize the importance of properly considering the effects of the Hubbard U and spin-orbit coupling to obtain the correct magnetic ground state. This study demonstrates accurate calculations of magnetic exchange constants for transition metal dihalides, which will help us to more deeply understand their magnetic properties and support further study of them.

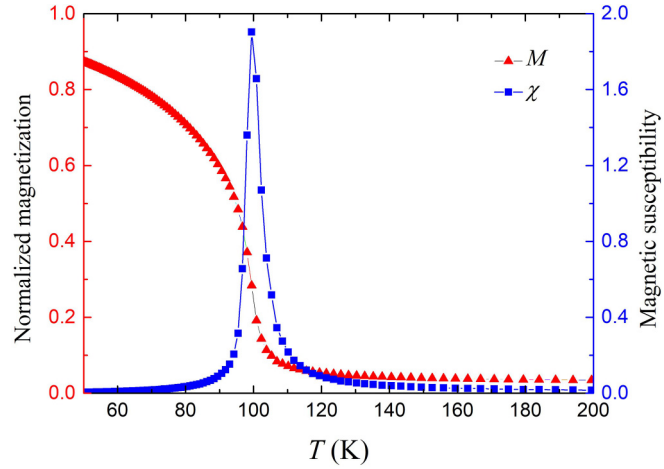

FIG. 4. Monte Carlo simulations of the magnetization and magnetic susceptibility for monolayer CrI_2.

ACKNOWLEDGMENTS

This work was supported by National Natural Science Foundation of China (Grants No. U1932159, No. 61874060, No. 61911530220, and No. 12104234), Jiangsu Specially-Appointed Professor Program, Natural Science Foundation of Jiangsu Province (Grants No. BK20181388 and No. BK20210578), Natural Science Foundation of Universities of Jiangsu Province (Grant No. 19KJA180007), Natural Science Foundation of Jiangsu Higher Education Institutions (Grant No. 20KJB140004), Jiangsu Provincial Double-Innovation Doctor Program (Grant No. JSSCBS20210513), Jiangsu Funding Program for Excellent Postdoctoral Talent (Grant No. 2022ZB401), and Natural Science Research Start-up Foundation of Recruiting Talents of Nanjing University of Posts and Telecommunications (Grant No. NY2211153).

[1] B. Huang, G. Clark, E. Navarro-Moratalla, D. R. Klein, R. Cheng, K. L. Seyler, D. Zhong, E. Schmidgall, M. A. McGuire, D. H. Cobden, W. Yao, D. Xiao, P. Jarillo-Herrero, and X. Xu, Layer-dependent ferromagnetism in a van der Waals crystal down to the monolayer limit, Nature (London) **546**, 270 (2017).

[2] C. Gong, L. Li, Z. Li, H. Ji, A. Stern, Y. Xia, T. Cao, W. Bao, C. Wang, Y. Wang, Z. Q. Qiu, R. J. Cava, S. G. Louie, J. Xia, and X. Zhang, Discovery of intrinsic ferromagnetism in two-dimensional van der Waals crystals, Nature (London) **546**, 265 (2017).

[3] Y. Deng, Y. Yu, Y. Song, J. Zhang, N. Z. Wang, Z. Sun, Y. Yi, Y. Z. Wu, S. Wu, J. Zhu, J. Wang, X. H. Chen, and Y. Zhang, Gate-tunable room-temperature ferromagnetism in two-dimensional Fe_3GeTe_2, Nature (London) **563**, 94 (2018).

[4] V. V. Kulish and W. Huang, Single-layer metal halides MX_2 (X = Cl, Br, I): Stability and tunable magnetism from first principles and Monte Carlo simulations, J. Mater. Chem. C **5**, 8734 (2017).

[5] S. Tomar, B. Ghosh, S. Mardanya, P. Rastogi, B. S. Bhadoria, Y. S. Chauhan, A. Agarwal, and S. Bhowmick, Intrinsic magnetism in monolayer transition metal trihalides: A comparative study, J. Magn. Magn. Mater. **489**, 165384 (2019).

[6] A. S. Botana and M. R. Norman, Electronic structure and magnetism of transition metal dihalides: Bulk to monolayer, Phys. Rev. Mater. **3**, 044001 (2019).

[7] X. Li, Z. Zhang, and H. Zhang, High throughput study on magnetic ground states with Hubbard U corrections in transition metal dihalide monolayers, Nanoscale Adv. **2**, 495 (2020).

[8] Z.-X. Shen, C. Su, and L. He, High-throughput computation and structure prototype analysis for two-dimensional ferromagnetic materials, npj Comput. Mater. **8**, 132 (2022).

[9] Z. Sun, H. Lv, Z. Zhuo, A. Jalil, W. Zhang, X. Wu, and J. Yang, A new phase of the two-dimensional ReS_2 sheet with tunable magnetism, J. Mater. Chem. C **6**, 1248 (2018).

[10] H. van Gog, W.-F. Li, C. Fang, R. S. Koster, M. Dijkstra, and M. van Huis, Thermal stability and electronic and magnetic properties of atomically thin 2D transition metal oxides, npj 2D Mater. Appl. **3**, 18 (2019).

[11] L. Liu, S. Chen, Z. Lin, and X. Zhang, A symmetry-breaking phase in two-dimensional $FeTe_2$ with ferromagnetism above room temperature, J. Phys. Chem. Lett. **11**, 7893 (2020).

[12] M. Yu, X. Liu, and W. Guo, Novel two-dimensional ferromagnetic semiconductors: Ga-based transition-metal trichalcogenide monolayers, Phys. Chem. Chem. Phys. **20**, 6374 (2018).

[13] X.-J. Dong, J.-Y. You, B. Gu, and G. Su, Strain-induced room-temperature ferromagnetic semiconductors with large anomalous Hall conductivity in two-dimensional $Cr_2Ge_2Se_6$, Phys. Rev. Appl. **12**, 014020 (2019).

[14] Y. Ren, Y. Ge, W. Wan, Q. Li, and Y. Liu, Two dimensional ferromagnetic semiconductor: Monolayer $CrGeS_3$, J. Phys.: Condens. Matter **32**, 015701 (2020).

[15] J.-Y. You, Z. Zhang, X.-J. Dong, B. Gu, and G. Su, Two-dimensional magnetic semiconductors with room Curie temperatures, Phys. Rev. Res. **2**, 013002 (2020).

[16] A. Kabiraj, M. Kumar, and S. Mahapatra, High-throughput discovery of high Curie point two-dimensional ferromagnetic materials, npj Comput. Mater. **6**, 35 (2020).

[17] X. Li, Y. Ge, J. Li, W. Wan, and Y. Liu, Electronic and magnetic properties of single-layer and double-layer VX_2 (X = Cl, Br) under biaxial stress, Chin. Phys. B **30**, 107305 (2021).

[18] J. Luo, G. Xiang, Y. Tang, K. Ou, and X. Chen, The electric and magnetic properties of novel two-dimensional $MnBr_2$ and MnI_2 from first-principles calculations, J. Appl. Phys. **128**, 113901 (2020).

[19] Y. Yang, P. Guo, and Y. Luo, Strain modulated ferromagnetic phase transitions in monolayer $FeCl_2$ through exchange competitions: The first-principle and Monte Carlo simulations, Phys. Chem. Chem. Phys. **22**, 17291 (2020).

[20] R. K. Ghosh, A. Jose, and G. Kumari, Intrinsic spin-dynamical properties of two-dimensional half-metallic FeX_2 (X = Cl, Br, I) ferromagnets: Insight from density functional theory calculations, Phys. Rev. B **103**, 054409 (2021).

[21] D. Amoroso, P. Barone, and S. Picozzi, Spontaneous skyrmionic lattice from anisotropic symmetric exchange in a Ni-halide monolayer, Nat. Commun. **11**, 5784 (2020).

[22] J. Y. Ni, X. Y. Li, D. Amoroso, X. He, J. S. Feng, E. J. Kan, S. Picozzi, and H. J. Xiang, Giant biquadratic exchange in 2D magnets and its role in stabilizing ferromagnetism of $NiCl_2$ monolayers, Phys. Rev. Lett. **127**, 247204 (2021).

[23] S. R. Kuindersma, J. P. Sanchez, and C. Haas, Magnetic and structural investigations on NiI_2 and CoI_2, Phys. B+C (Amsterdam) **111**, 231 (1981).

[24] T. Kurumaji, S. Seki, S. Ishiwata, H. Murakawa, Y. Kaneko, and Y. Tokura, Magnetoelectric responses induced by domain rearrangement and spin structural change in triangular-lattice helimagnets NiI_2 and CoI_2, Phys. Rev. B **87**, 014429 (2013).

[25] H. Ju, Y. Lee, K.-T. Kim, I. H. Choi, C. J. Roh, S. Son, P. Park, J. H. Kim, T. S. Jung, J. H. Kim, K. H. Kim, J.-G. Park, and J. S. Lee, Possible persistence of multiferroic order down to bilayer limit of van der Waals material NiI_2, Nano Lett. **21**, 5126 (2021).

[26] Q. Song, C. A. Occhialini, E. Ergeçen, B. Ilyas, D. Amoroso, P. Barone, J. Kapeghian, K. Watanabe, T. Taniguchi, A. S. Botana, S. Picozzi, N. Gedik, and R. Comin, Evidence for a single-layer van der Waals multiferroic, Nature (London) **602**, 601 (2022).

[27] A. O. Fumega and J. L. Lado, Microscopic origin of multiferroic order in monolayer NiI_2, 2D Mater. **9**, 025010 (2022).

[28] M. Lu, Q. Yao, C. Xiao, C. Huang, and E. Kan, Mechanical, electronic, and magnetic properties of NiX_2 (X = Cl, Br, I) layers, ACS Omega **4**, 5714 (2019).

[29] E. Torun, H. Sahin, S. K. Singh, and F. M. Peeters, Stable half-metallic monolayers of $FeCl_2$, Appl. Phys. Lett. **106**, 192404 (2015).

[30] M. Ashton, D. Gluhovic, S. B. Sinnott, J. Guo, D. A. Stewart, and R. G. Hennig, Two-dimensional intrinsic half-metals with large spin gaps, Nano Lett. **17**, 5251 (2017).

[31] X. Zhou, B. Brzostowski, A. Durajski, M. Liu, J. Xiang, T. Jiang, Z. Wang, S. Chen, P. Li, Z. Zhong, A. Drzewiński, M. Jarosik, R. Szczęśniak, T. Lai, D. Guo, and D. Zhong, Atomically thin 1T-$FeCl_2$ grown by molecular-beam epitaxy, J. Phys. Chem. C **124**, 9416 (2020).

[32] S. Cai, F. Yang, and C. Gao, $FeCl_2$ monolayer on HOPG: Art of growth and momentum filtering effect, Nanoscale **12**, 16041 (2020).

[33] D. Lu, L. Liu, Y. Ma, K. Yang, and H. Wu, Unique electronic state in ferromagnetic semiconductor $FeCl_2$ monolayer, J. Mater. Chem. C **10**, 8009 (2022).

[34] A. I. Liechtenstein, M. I. Katsnelson, V. P. Antropov, and V. A. Gubanov, Local spin density functional approach to the theory

of exchange interactions in ferromagnetic metals and alloys, J. Magn. Magn. Mater. **67**, 65 (1987).
[35] X. Wan, Q. Yin, and S. Y. Savrasov, Calculation of magnetic exchange interactions in Mott-Hubbard systems, Phys. Rev. Lett. **97**, 266403 (2006).
[36] X. Wan, T. A. Maier, and S. Y. Savrasov, Calculated magnetic exchange interactions in high-temperature superconductors, Phys. Rev. B **79**, 155114 (2009).
[37] D. Wang, X. Bo, F. Tang, and X. Wan, First-principles study of the spin-orbit coupling contribution to anisotropic magnetic interactions, Phys. Rev. B **108**, 085140 (2023).
[38] P. Blaha, K. Schwarz, G. K. Madsen, D. Kvasnicka, and J. Luitz, *WIEN2k, An Augmented Plane Wave + Local Orbitals Program for Calculating Crystal Properties* (Technische Universitt Wien, Vienna, 2001).
[39] V. I. Anisimov, F. Aryasetiawan, and A. I. Lichtenstein, First-principles calculations of the electronic structure and spectra of strongly correlated systems: The LDA $+U$ method, J. Phys.: Condens. Matter **9**, 767 (1997).
[40] See Supplemental Material at http://link.aps.org/supplemental/10.1103/PhysRevB.109.014405 for computational details and some additional results, which includes Refs. [63–72].
[41] D. D. Koelling and B. N. Harmon, A technique for relativistic spin-polarised calculations, J. Phys. C: Solid State Phys. **10**, 3107 (1977).
[42] H. Xiang, C. Lee, H.-J. Koo, X. Gong, and M.-H. Whangbo, Magnetic properties and energy-mapping analysis, Dalton Trans. **42**, 823 (2013).
[43] R. E. Prange and V. Korenman, Local-band theory of itinerant ferromagnetism. IV. Equivalent Heisenberg model, Phys. Rev. B **19**, 4691 (1979).
[44] C. S. Wang, R. E. Prange, and V. Korenman, Magnetism in iron and nickel, Phys. Rev. B **25**, 5766 (1982).
[45] V. P. Antropov, The exchange coupling and spin waves in metallic magnets: Removal of the long-wave approximation, J. Magn. Magn. Mater. **262**, L192 (2003).
[46] I. V. Solovyev, Exchange interactions and magnetic force theorem, Phys. Rev. B **103**, 104428 (2021).
[47] X. Wan, J. Dong, and S. Y. Savrasov, Mechanism of magnetic exchange interactions in europium monochalcogenides, Phys. Rev. B **83**, 205201 (2011).
[48] D. Wang, X. Bo, F. Tang, and X. Wan, Calculated magnetic exchange interactions in the Dirac magnon material Cu_3TeO_6, Phys. Rev. B **99**, 035160 (2019).
[49] X. Bo, D. Wang, B. Wan, and X. G. Wan, Calculated magnetic exchange interactions in the quantum spin chain materials $K_2CuSO_4Cl_2$ and $K_2CuSO_4Br_2$, Phys. Rev. B **101**, 024416 (2020).
[50] X. Wan, V. Ivanov, G. Resta, I. Leonov, and S. Y. Savrasov, Exchange interactions and sensitivity of the Ni two-hole spin state to Hund's coupling in doped $NdNiO_2$, Phys. Rev. B **103**, 075123 (2021).
[51] Z.-X. Shen, X. Bo, K. Cao, X. Wan, and L. He, Magnetic ground state and electron-doping tuning of Curie temperature in Fe_3GeTe_2 : First-principles studies, Phys. Rev. B **103**, 085102 (2021).
[52] X. Bo, F. Li, X. Xu, X. Wan, and Y. Pu, Calculated magnetic exchange interactions in the van der Waals layered magnet CrSBr, New J. Phys. **25**, 013026 (2023).
[53] X. Bo, F. Li, X. Yin, Y. Chen, X. Wan, and Y. Pu, Magnetic structure and exchange interactions of the van der Waals $CrPS_4$ monolayer under strain: A first-principles study, Phys. Rev. B **108**, 024405 (2023).
[54] D. Wang, X. Bo, F. Tang, and X. Wan, WienJ, https://github.com/diwang0214/WienJ.
[55] K. Cao, G.-C. Guo, D. Vanderbilt, and L. He, First-principles modeling of multiferroic RMn_2O_5, Phys. Rev. Lett. **103**, 257201 (2009).
[56] K. Shirali, W. A. Shelton, and I. Vekhter, Importance of van der Waals interactions for *ab initio* studies of topological insulators, J. Phys.: Condens. Matter **33**, 035702 (2020).
[57] Q. Yao, J. Li, and Q. Liu, Fragile symmetry-protected half metallicity in two-dimensional van der Waals magnets: A case study of monolayer $FeCl_2$, Phys. Rev. B **104**, 035108 (2021).
[58] A. Kartsev, M. Augustin, R. F. L. Evans, K. S. Novoselov, and E. J. G. Santos, Biquadratic exchange interactions in two-dimensional magnets, npj Comput. Mater. **6**, 150 (2020).
[59] C. D. Batista, S.-Z. Lin, S. Hayami, and Y. Kamiya, Frustration and chiral orderings in correlated electron systems, Rep. Prog. Phys. **79**, 084504 (2016).
[60] S. Hayami, S.-Z. Lin, and C. D. Batista, Bubble and skyrmion crystals in frustrated magnets with easy-axis anisotropy, Phys. Rev. B **93**, 184413 (2016).
[61] J. Liu, Q. Sun, Y. Kawazoe, and P. Jena, Exfoliating biocompatible ferromagnetic Cr-trihalide monolayers, Phys. Chem. Chem. Phys. **18**, 8777 (2016).
[62] A. Kartsev, O. D. Feya, N. Bondarenko, and A. G. Kvashnin, Stability and magnetism of FeN high-pressure phases, Phys. Chem. Chem. Phys. **21**, 5262 (2019).
[63] G. Kresse and J. Hafner, *Ab initio* molecular dynamics for liquid metals, Phys. Rev. B **47**, 558(R) (1993).
[64] G. Kresse and J. Furthmüller, Efficient iterative schemes for *ab initio* total-energy calculations using a plane-wave basis set, Phys. Rev. B **54**, 11169 (1996).
[65] P. E. Blöchl, Projector augmented-wave method, Phys. Rev. B **50**, 17953 (1994).
[66] G. Kresse and D. Joubert, From ultrasoft pseudopotentials to the projector augmented-wave method, Phys. Rev. B **59**, 1758 (1999).
[67] J. Heyd, G. E. Scuseria, and M. Ernzerhof, Hybrid functionals based on a screened Coulomb potential, J. Chem. Phys. **118**, 8207 (2003).
[68] L. Passell, O. W. Dietrich, and J. Als-Nielsen, Neutron scattering from the Heisenberg ferromagnets EuO and EuS. I. The exchange interactions, Phys. Rev. B **14**, 4897 (1976).
[69] K. B. Lyons, P. A. Fleury, J. P. Remeika, A. S. Cooper, and T. J. Negran, Dynamics of spin fluctuations in lanthanum cuprate, Phys. Rev. B **37**, 2353 (1988).
[70] M. Hälg, W. E. A. Lorenz, K. Y. Povarov, M. Månsson, Y. Skourski, and A. Zheludev, Quantum spin chains with frustration due to Dzyaloshinskii-Moriya interactions, Phys. Rev. B **90**, 174413 (2014).
[71] A. Scheie, M. Ziebel, D. G. Chica, Y. J. Bae, X. Wang, A. I. Kolesnikov, X. Zhu, and X. Roy, Spin waves and magnetic exchange Hamiltonian in CrSBr, Adv. Sci. **9**, 2202467 (2022).
[72] S. Calder, A. V. Haglund, Y. Liu, D. M. Pajerowski, H. B. Cao, T. J. Williams, V. O. Garlea, and D. Mandrus, Magnetic structure and exchange interactions in the layered semiconductor $CrPS_4$, Phys. Rev. B **102**, 024408 (2020).